Preferential binding of a kinesin-1 motor to GTP-tubulin–rich microtubules underlies polarized vesicle transport

Takao Nakata,[1,2] Shinsuke Niwa,[1] Yasushi Okada,[1] Franck Perez,[3] and Nobutaka Hirokawa[1]

[1]Department of Cell Biology and Anatomy, Graduate School of Medicine, the University of Tokyo, 7-3-1 Hongo, Tokyo 113-0033, Japan
[2]Department of Cell Biology, Graduate School of Medicine, Tokyo Medical and Dental University, 1-5-45 Yushima, Tokyo 113-8510, Japan
[3]Institut Curie, Centre National de la Recherche Scientifique, UMR144 26, F-75248, Paris Cedex 05, France

Polarized transport in neurons is fundamental for the formation of neuronal circuitry. A motor domain–containing truncated KIF5 (a kinesin-1) recognizes axonal microtubules, which are enriched in EB1 binding sites, and selectively accumulates at the tips of axons. However, it remains unknown what cue KIF5 recognizes to result in this selective accumulation. We found that axonal microtubules were preferentially stained by the anti–GTP-tubulin antibody hMB11. Super-resolution microscopy combined with EM immunocytochemistry revealed that hMB11 was localized at KIF5 attachment sites. In addition, EB1, which binds preferentially to guanylyl-methylene-diphosphate (GMPCPP) microtubules in vitro, recognized hMB11 binding sites on axonal microtubules. Further, expression of hMB11 antibody in neurons disrupted the selective accumulation of truncated KIF5 in the axon tips. In vitro studies revealed approximately threefold stronger binding of KIF5 motor head to GMPCPP microtubules than to GDP microtubules. Collectively, these data suggest that the abundance of GTP-tubulin in axonal microtubules may underlie selective KIF5 localization and polarized axonal vesicular transport.

Introduction

Polarized distribution of membrane proteins is necessary for neurons to transmit information to their targets. Polarized transport plays an important role in the compartmentalization of membrane proteins. Indeed, dendrite membrane proteins are mainly transported within somatodendrites in mature neurons (Burack et al., 2000), and axonal membrane proteins are directly transported from the Golgi region to the axons via tubular–vesicular organelles (Nakata et al., 1998; Nakata and Hirokawa, 2003). Polarized transport in neurons has been studied through the dissociated culture of rodent hippocampal neurons (Goslin and Banker, 1999). After plating, neurons extend several undifferentiated neurites (stages 1–2). Then, one process begins to grow rapidly and becomes an axon, whereas the others remain short and become dendrites (stage 3). Until this stage, microtubule (MT) polarity is plus-end outward in both axons and dendrites (Baas et al., 1989). The axon and dendrites gradually reach maturation, acquiring their individual characteristics, such as pre- and postsynaptic structures (stages 4–5). After these stages, MT polarity in the cell body and proximal dendrites becomes mixed, remaining plus-end outward in axons and distal dendrites (Baas et al., 1989).

MT-based motor proteins, kinesin superfamily proteins (KIFs), and dyneins play an important role in intracellular transport (Hirokawa and Takemura, 2005; Hirokawa et al., 2010). They interact with MTs via their motor domains and move toward either the plus end or minus end of MTs, according to their motor head properties. N-terminal KIFs such as KIF5 (kinesin-1) and KIF1A (kinesin-3) are plus end–directed motors, whereas dyneins and C-terminal KIFs are minus end–directed motors. Their tail domains interact with their cargoes. Previously, we showed that truncated KIF5 accumulated specifically at the tips of axons (Nakata and Hirokawa, 2003), and this was later confirmed in stage 3 neurons (Jacobson et al., 2006). Truncated KIF5 is free from self-inhibition by its tail domain, and is considered to be constitutively active (Coy et al., 1999;

Correspondence to Nobutaka Hirokawa: hirokawa@m.u-tokyo.ac.jp

Abbreviations used in this paper: CCD, charge-coupled device; GMPCPP, guanylyl-methylene-diphosphate; KIF, kinesin superfamily protein; MAP, microtubule-associated protein; MT, microtubule; TIRF, total internal reflection fluorescence.

The Rockefeller University Press $30.00
J. Cell Biol. Vol. 194 No. 2 245–255
www.jcb.org/cgi/doi/10.1083/jcb.201104034

Friedman and Vale, 1999). The most straightforward interpretation of its distribution is that the KIF5 motor domain preferentially chooses axonal MTs as a track and moves along them (Nakata and Hirokawa, 2003). However, the molecular nature of the directional cue on axonal MTs remains unknown.

Using various approaches, including immunostaining, and an in vitro motor binding assay, expression of an antibody specific for GTP-tubulin, and dual-color super-resolution microscopy, we found evidence supporting a role for GTP-tubulin as the axonal cue. These results may fill previous gaps in our knowledge and may provide a broader view of the mechanism underlying polarized vesicular transport in neurons.

Results

Previously known tubulin modifications and MAP2 are not the axonal cue

To study the molecular mechanism by which truncated KIF5 recognizes axonal MTs, we first made chimeric motor heads of KIF5C (K381-YFP) and KIF1A (C381-YFP; Fig. 1). A truncated dimer of the KIF5 motor heads accumulated specifically at axonal tips, whereas a truncated dimer of KIF1A motor heads (C381-YFP) accumulated at both axon and dendrite tips, as described previously (Jacobson et al., 2006). We exchanged three major MT-binding domains in KIFs—loop 8, loop 11, and loop 12—between KIF5C and KIF1A, and observed the behavior of the resultant chimeric proteins in neurons for 8 h by time-lapse video. When loop 8 was exchanged, C381 (C8A) showed diffuse distribution, which suggests that its motility was lost, whereas targeting of K381 (K8R) was unchanged. When loop 12 was exchanged, targeting of C381 was changed moderately (CK1), whereas the targeting of K381-YFP (SK2) was unchanged. In contrast, when loop 11 was exchanged, truncated KIF5C containing loop 11 of KIF1A (K11C) tended to accumulate at multiple tips, whereas truncated KIF1A containing loop 11 of KIF5C (C11K) showed diffuse distribution like C8A, which suggests that its motility was lost (or had low motor efficacy; Song et al., 2009). Recently, β5–loop 8 mutant of KIF5 was found to localize in dendrites (Konishi and Setou, 2009). The discrepancy may be attributed to a low motor efficacy of the β5–loop 8 mutant because the mutant appears to distribute throughout the somatodendritic area with most in the cell body, instead of accumulating at the tips of dendrites as seen with C-381 (Fig. 1).

Our previous in vitro binding experiments with the same loop chimeras (Okada and Hirokawa 2000) showed that the loop 8 chimera affected MT affinity throughout the ATPase cycle, whereas the loop 11 chimera mainly affected the strong binding states (Apo to ATP states) and the loop 12 chimera mainly affected the weak binding states (ADP states). These biochemical results are consistent with the structure (Nitta et al., 2004). Loop 8 is located at the center of the MT-binding surface of kinesin, and loops 11 and 12 extend from opposite sides of kinesin. Loop 11 is extended deeply into the tubulin monomer cleft in the ATP state, whereas loop 12 extends to the surface C-terminal end of tubulin in the ADP state. Thus, massive mutations in loop 8 (such as in the β5–loop 8 mutant) might severely damage the microtubule-binding surface, leading to low motor efficacy. The loop 12–tubulin interaction in the ADP state has been shown to be related to processivity, the mean run length before full detachment of kinesin. Our results suggest that this interaction does not play an important role in MT discrimination. On the contrary, the interaction mediated by loop 11 has been suggested to play a pivotal role in MT discrimination. Our in vivo and in vitro results showed that MT discrimination occurs in the strong binding states (Apo or ATP state), when loop 11 is extended to the cleft between tubulin monomers. Loop 11 might thus sense putative structural changes in tubulin accompanied by GTP hydrolysis.

Next, we examined the localization of tyrosinated, detyrosinated, polyglutaminated, and acetylated MTs in neurons (Fig. S1) because posttranslational modifications of tubulin, such as acetylation (Reed et al., 2006; Cai et al., 2009; Tapia et al., 2010; Friedman et al., 2010) and tyrosination (Konishi and Setou, 2009), are primary candidates for axonal (or dendritic) cues on MTs (Hammond et al., 2008). We may say that modified MTs are abundant in axons if they are more abundant in the axon than in the average dendrite, even if they are less abundant in the axon than those in the top dendrite, of the same neuron. However, as a directional cue, modified MTs should be most abundant in the axon among all the neurites (axon plus dendrites) for KIF5 to accumulate at the tips of axons. This was not always the case in acetylated MTs (Fig. S1, A and E). Application of trichostatin A, an HDAC6 inhibitor, increased the amount of acetylated tubulin in non-neural cells but did not perturb axonal localization of K381 (Fig. S2). Tyrosinated, detyrosinated, and polyglutaminated MTs were localized in both proximal dendrites and the initial segments of axons (Fig. S1, B–E), and their expression levels were similar between proximal dendrites and initial segments of axons. Tyrosinated tubulin was not crucial for axonal outgrowth, as seen in tubulin–tyrosine–ligase (TTL) knockout mice in vivo (Marcos et al., 2009). The localization patterns of these modified tubulins suggested that none alone was the exclusive directional cue, although they could be partially involved in the cue (Hammond et al., 2010). Indeed, the same question was addressed 20 yr ago in the context of whether tubulin modifications could be an axonal (or dendritic) marker in hippocampal neurons (Dotti and Banker, 1991).

Among microtubule-associated proteins (MAPs), MAP2 and tau have widely been used as dendrite and axonal markers. Although tau protein itself localizes to both axons and dendrites (the axonal marker tau-1 antibody recognizes phosphorylated tau protein, which is dominant in distal axons), MAP2 shows clear somatodendritic localization. Single tau knockout mice developed neurons which were functionally and structurally almost normal (Takei et al., 2000). Thus, we tested whether MAP2 could be the spatial cue for truncated KIF5. However, truncated KIF5 accumulated only in the axons of MAP2-null neurons at stage 3, which indicates that MAP2 was not a spatial cue for KIF5 (Video 1). Although a combination of these known MT properties might be the axonal cue, these results prompted us to seek a novel feature of axonal MTs as the possible cue.

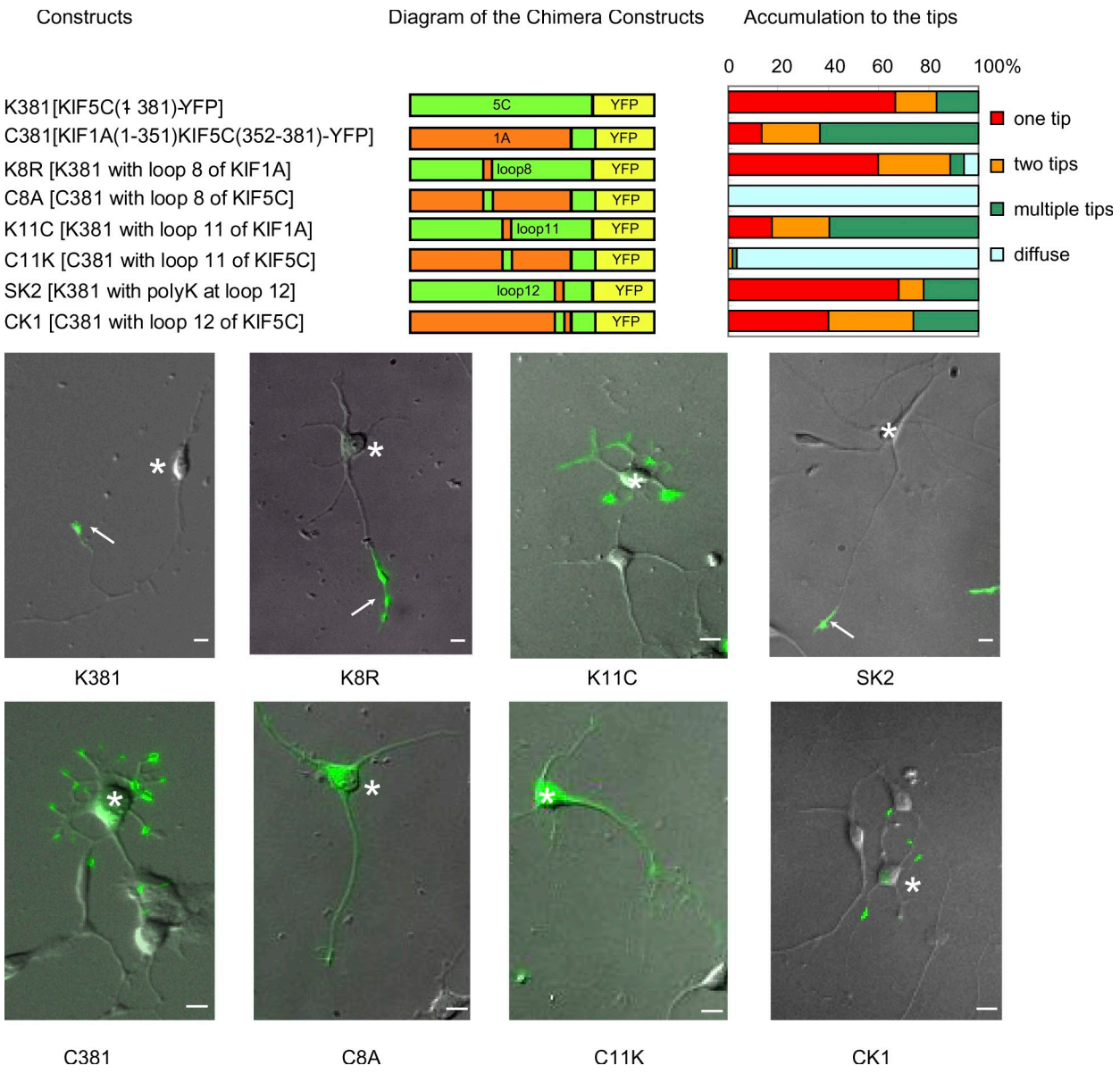

Figure 1. **KIF5 motor head domain for axonal preference.** Chimeric proteins of KIF1A (C381) and KIF5C (K381) were expressed in stage 3 neurons. Neurons were classified based on the numbers of neurites that accumulated the chimera at their tips, and their percentages among all neurons are shown in the graph. One tip corresponds to the selective accumulation in axons. Bottom panels show representative images of neurons expressing each construct. YFP images were superimposed on differential interference contrast microscopy images. Arrows indicate the tips of axons and asterisks indicate the cell bodies of transfected neurons. Bars, 10 µm.

hMB11 antibody preferentially stains axonal MTs

Recently, an antibody (hMB11) that specifically recognizes GTP-tubulin was developed using phage display screening. The antibody stained not only the growing tips of MTs, the GTP caps, but also spots located randomly along the MTs (GTP remnants) in various cell lines (Dimitrov et al., 2008). We found that the hMB11 antibody extensively stained axonal MTs in cultured hippocampal neurons (Fig. 2, A and B). At stage 2, biased staining of some neurites was already seen in some neurons (Fig. 2 A). At stage 3, the proximal area of the axon was most stained among other neurites (Fig. 2 A, arrow). At stage 4, biased axonal staining was clear among the dendrites (Fig. 2 B, arrows). This does not necessarily mean that dendrite MTs were not stained, but the staining pattern was highly biased. Previously, we have shown that treatment with 10 nM taxol diminishes neuronal polarity (Nakata and Hirokawa, 2003). Thus, spatial cues in axons need to be changed by this treatment. Consistent with this criterion, the axon-preferential staining pattern of hMB11 was diminished by 10 nM taxol treatment (Fig. 2 C). The hMB11 staining pattern matches the requirements for the axonal cue. Axonal enrichment of GTP-MTs is supported by the following independent evidence. Recently, EB1-GFP was shown to have higher affinity to GTP-MTs than to GDP-MTs in vitro (Zanic et al., 2009). We found that the distribution of EB1-GFP depends on its expression level in neurons. At low expression levels, EB1 was localized at the tips of growing MTs in both axons and somatodendrites. However, at slightly higher

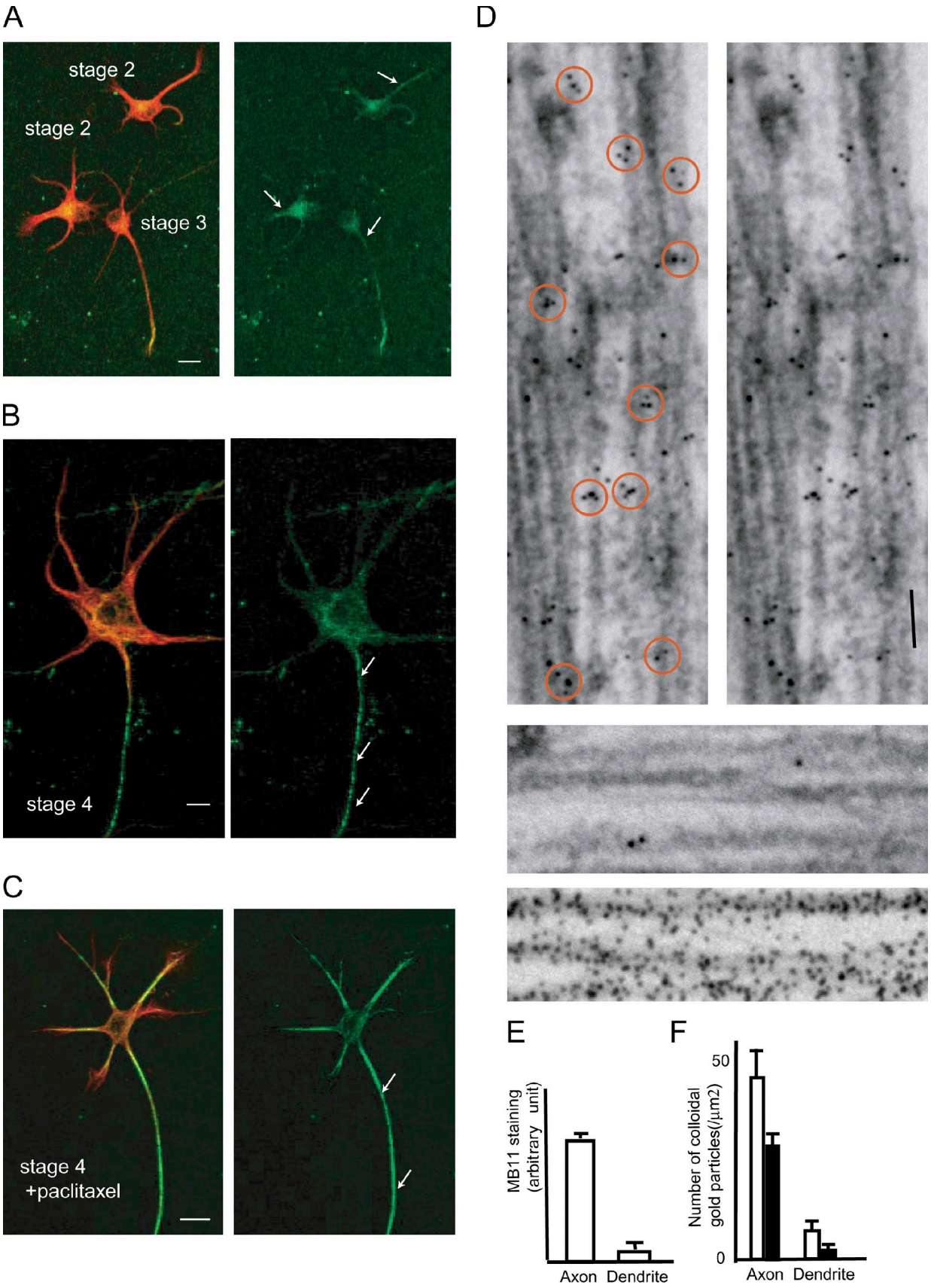

Figure 2. **hMB11 staining in neurons.** (A and B) Staining with hMB11antibody of GTP-tubulin (green) at stage 2–3 (A) and stage 4 (B). Cells were counterstained with anti-MAP2 antibody (red). At stage 2, the hMB11 stain was biased among neurites (arrows). At stage 3, hMB11 stains the axon (arrow). (C) 100 nM paclitaxel was added. Note that paclitaxel treatment caused accumulation of GTP-tubulin in both axons and dendrites. Bars, 10 μm. (D, top) Double-label immunoelectron microscopy of axons with EB1 (10 nm) and hMB11 (5 nm). Orange circles on the left indicate patchy localization

expression levels, EB1 fully decorated axonal MTs, whereas it bound only to the tips of growing MTs in somatodendrites of the same neuron (Nakata and Hirokawa, 2003). Although this distribution represents an artificial condition, this finding clearly demonstrates a difference between axonal and dendritic MTs. Therefore, we tested whether hMB11 and EB1-YFP (at high dose) recognize the same structure on axonal MTs by immunoelectron microscopy. In our permeabilization condition for hMB11, although EB1-YFP comets disappeared from the growing tips of MTs, EB1-YFP remained on the axonal MTs. We found that EB1 and hMB11 staining colocalized as patches on axonal MTs (Fig. 2 D, top), but not on dendritic MTs (Fig. 2 D, middle). An α-tubulin antibody (DM1A) showed diffuse labeling (Figs. 2 D, bottom). Similar to hMB11 staining, 10 nM taxol changed the axon-specific localization of EB1-YFP (Nakata and Hirokawa, 2003). These results indicate that hMB11 and EB1 both recognize a structure abundant in axonal MTs, probably GTP remnants.

Super-resolution microscopy revealed colocalization of hMB11 staining and KIF5 binding sites

Because of their biased localization in axons, we tested whether the structure recognized by hMB11 antibody was the axonal cue for polarized axonal transport. First, we tested the relationship between hMB11 and KIF5 binding sites in axons. Confocal microscopy using an α-plan-fluor objective lens (100×, 1.45 NA) suggested axon-dominant and clustered hMB11 staining. However, clustered staining of hMB11 was unclear because of the diffraction limit of light (Fig. S3, A and B). Thus, we took advantage of super-resolution microscopy using blinking of ATTO dyes (van de Linde et al., 2009). This gave higher resolution compared with conventional microscopy (Fig. S3 C). In neurons, we could clearly discriminate clustered hMB11 staining that was more abundant in axons than dendrites (Fig. 3 A). In contrast, the α-tubulin staining pattern was smoother than the hMB11 staining pattern, and did not show polarized distribution (Fig. 3 B). The localization precision of ATTO565 was ∼15 nm in these figures (Fig. S4 D). Although the resolution was much higher, these images were consistent with images taken by confocal microscopy, excluding the possibility that clustered staining of hMB11 is an artifact of super-resolution microscopy (Figs. 2 and S3, A and B). To observe the relationship of motors with hMB11-positive structures using super-resolution microscopy, the motor domains of KIF5 (K381) and KIF1A (C381) were fused with Dronpa (Ando et al., 2004), a photoswitchable fluorescent protein that can be used for super-resolution microscopy (Betzig et al., 2006). Neurons were transfected by adenoviruses encoding these proteins, permeabilized by 0.01% saponin in the presence 5 mM AMP-PNP and hMB11, stained by ATTO565-labeled anti–human IgG antibody, and observed by super-resolution microscopy. As a result, clusters of KIF5 motor domain were well colocalized with hMB11-positive clusters (Fig. 3 C). Quantification revealed that 73.4 ± 12.2% of truncated KIF5-positive clusters localized on hMB11 clusters (mean ± SD, n = 230, from five independent samples), whereas 35.4 ± 12.3% of truncated KIF1A-positive clusters localized on hMB11 clusters (mean ± SD, n = 184, from five independent samples). To exclude the possibility that experimental procedures affected hMB11 staining, we quantified the density of hMB11 staining along MTs in control cells, EB1-expressing cells, and motor domain–expressing and AMP-PNP–treated cells using super-resolution microscopy. The results suggested that our experimental procedures did not affect hMB11 staining (Fig. S3 E). Similar to hMB11 staining, treatment with low-dose paclitaxel alters the distribution of truncated KIF5 (Nakata and Hirokawa, 2003). The results indicated that truncated KIF5 was preferentially recruited to the GTP-tubulin–rich domain on axonal MTs.

Dynamics of truncated KIF5C-YFP in neurons expressing hMB11-mCherry

Second, we disrupted accumulation of truncated KIF5C-YFP in axonal tips by overexpressing recombinant hMB11 tagged with a fluorescent protein (hMB11-mCherry) in living cultured neurons. We expressed both truncated KIF5C and hMB11-mCherry in stage 2 neurons. Initially, truncated KIF5C-YFP accumulated to the tips of neurites because their motor activity overrides their diffusion (Fig. 4 A, green, 460–610 min). In contrast, as hMB11 binds to GTP-MTs but does not have motor activity, its localization is subject to the balance among its synthesis in the cell body, diffusion, and binding to the antigen. Indeed, hMB11 was localized mainly in the cell body and the proximal area of the same neurites in the tips of which truncated KIF5-YFP accumulated. In contrast, truncated KIF1A accumulated in multiple tips, whereas hMB11-mCherry localized to mainly one or two neurites at a time (Fig. S4). When the expression level of hMB11-mCherry was high (Fig. 4 A, green, 730 min), truncated KIF5 failed to accumulate in the tips of neurites (Fig. 4 A, green, 730 min). This was quantified by measuring the expression of MB11-mCherry in the cell body, and the localization of truncated KIF5C-YFP in hMB11-mCherry and truncated KIF5C-GFP double-transfected cells (Fig. 4 B), which indicates that truncated KIF5 localization was disrupted in neurons expressing high levels of hMB11-mCherry.

KIF5 motor heads preferentially bind to GMPCPP-MTs in vitro

We performed an in vitro assay of KIF5C binding to GTP-MTs and GDP-MTs to directly and quantitatively show its higher

of 5-nm and 10-nm gold on MTs. The right shows the same view without circles. The middle shows the dendrite domain of the same neuron. The bottom shows control staining with a pan-MT antibody (DM1A; 10 nm colloidal gold). (E) Quantification of the axonal and dendritic staining of MB11 at stage 4. For dendrite staining, the highest fluorescence intensity was measured in dendrites (n = 72). For axonal staining, the highest fluorescence intensity was measured between the cell body and the axonal position at the same distance from the cell body with adjacent dendrites. Error bars indicate SEM. (F) Quantification of D. The number of 5-nm and 10-nm colloidal gold particles per axonal and dendrite area was counted (white column, 10 nm; black column, 5 nm). n = 14 (axons) and n = 6 (dendrites).

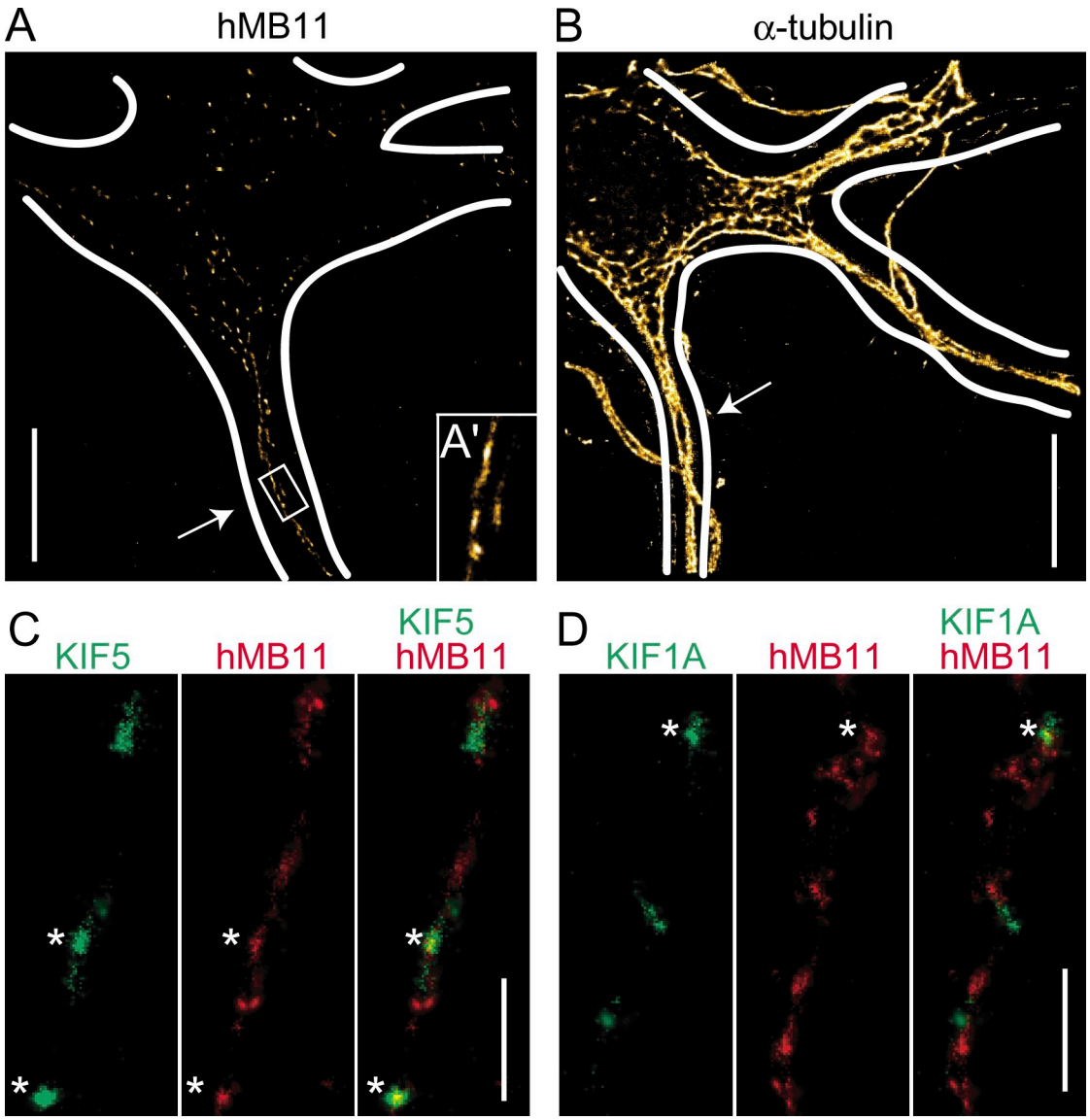

Figure 3. **Super-resolution microscopy of GTP-tubulin clusters and KIF5 binding sites in axonal MTs of stage 4 hippocampal neurons.** (A, A′, and B) Reconstructed super-resolution microscopy images of hMB11 staining (A and A′) and anti–α-tubulin antibody staining (B) followed by ATTO565-labeled secondary antibodies. A′ shows a magnification of the boxed area in A. Note that hMB11 staining was more abundant in axons (arrows), whereas α-tubulin staining was not polarized. Bars, 25 µm. (C and D) Motor domain binding sites in axons. KIF5 binding sites (C) and KIF1A binding sites (D). Dronpa-fused motors (green) and hMB11 staining (red) were observed. Colocalization is indicated by asterisks. Bars, 2 µm.

affinity for GTP-MTs. We polymerized fluorescently labeled GMPCPP-MTs (mimicking GTP-MTs) and GDP-MTs, mixed them, and added different concentrations of fluorescently labeled KIF5C motor head (Fig. 5). At high KIF5C concentration (>1,000 nM), KIF5C motor head was bound to both GMPCPP-MTs and GDP-MTs. However, at lower KIF5C concentrations, KIF5C was preferentially bound to GMPCPP-MTs (Fig. 5, A and B). Quantitative analysis (Fig. 5 C) revealed that the affinity of KIF5C motor head for GTP-MTs was 3.7 times higher (K_{diss} = 250 ± 90 nM) than that for GDP-MTs (K_{diss} = 930 ± 250 nM). The affinity for GDP-MTs estimated here is in good agreement with the previously reported value (1,100 ± 110 nM) for GDP-taxol MTs (Rosenfeld et al., 1996), which suggests that GMPCPP-MTs are a better substrate for KIF5C, which is consistent with the findings of the previous in vitro motility assay (Vale et al., 1994). These results directly demonstrate that KIF5C motor head can discriminate the MT lattice structures with different guanine nucleotide contents.

Discussion

We set out to identify the directional cue on axonal MTs that causes a biased accumulation of truncated KIF5 to axonal tips. Posttranslational modification of tubulins and MT-associated proteins were possible candidates for the cue. In addition, we found a novel feature of axonal MTs, which is that they are rich in GTP-MTs, and we tested this feature as a possible directional cue.

We initially tested previously known features of neuronal MTs, such as tubulin posttranslational modifications

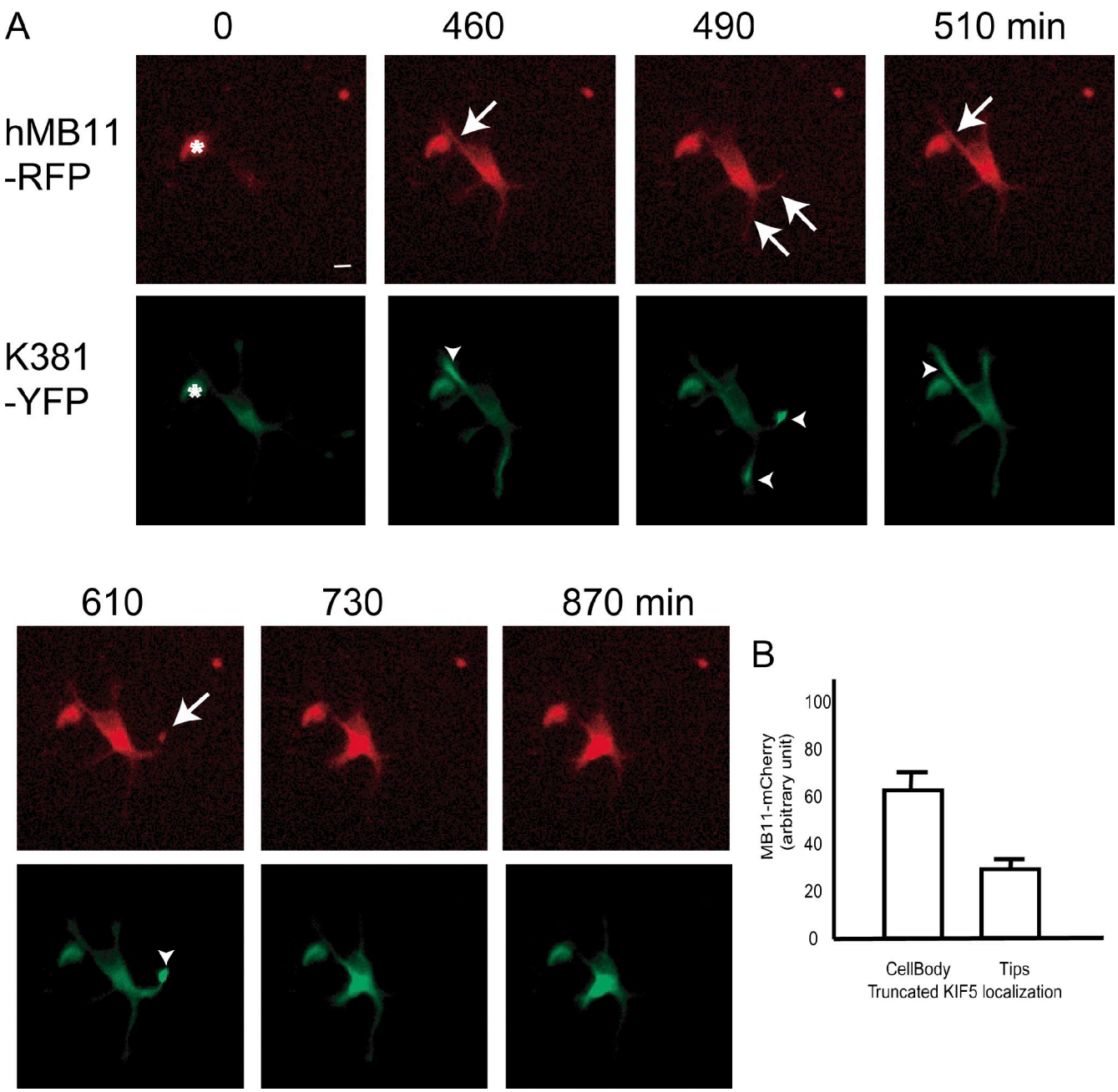

Figure 4. **Disruption of axonal accumulation of KIF5C by high-level expression of hMB11-mCherry.** (A) hMB11-mCherry was initially dimly expressed around the cell body (0 min, red), but gradually covered whole neurons (arrow, 490 min, red). The asterisk at 0 min indicates cell debris. Truncated KIF5 (green), which initially accumulated at the tip of the axon (arrowheads, 460–610 min, green), went back into the cell body (730, 870 min, green). Images were enhanced to visualize neurites and, accordingly, cell body staining was saturated after 490 min. The intensity of original images of cell body staining of hMB11-RFP was 32 (460 min), 46 (510 min), and 86 (730 min) in arbitrary units. Bar, 20 µm. (B) Quantification of hMB11-mCherry expression level and localization of truncated KIF5 in stage 3 neurons (n = 55). hMB11 level in the cell body was quantified. Error bars indicate SEM. Bars, 10 µm.

(Hammond et al., 2010). However, careful examination of the distribution of these modifications in neurons revealed that their bias alone was not sufficient to explain the exclusive localization of truncated KIF5 at axonal tips, and there is a possibility that previously unknown cues are involved (Fig. S1). Truncated KIF5 is specifically targeted to axons in MAP2-null neurons (Video 1). Therefore, although it might be possible that a mixture of these modifications influences truncated KIF5 localization, we sought a previously unknown structural difference between axonal and dendritic MTs.

The recombinant antibody hMB11 stained axonal MTs far more brightly than dendritic MTs (Fig. 2). hMB11 recognizes a GTP-bound form of tubulin in vitro and in nonneuronal cells (Dimitrov et al., 2008), which suggests that the difference in hMB11 staining might be attributed to a difference in the abundance of GTP-tubulin patches between axonal and dendritic MTs. It has been generally assumed that GTP-MTs are confined to a few subunits at the ends of growing MTs (GTP-cap). However, this was based on biochemical analysis of MT assembly in vitro, and there is little direct evidence of the nucleotide form or atomic

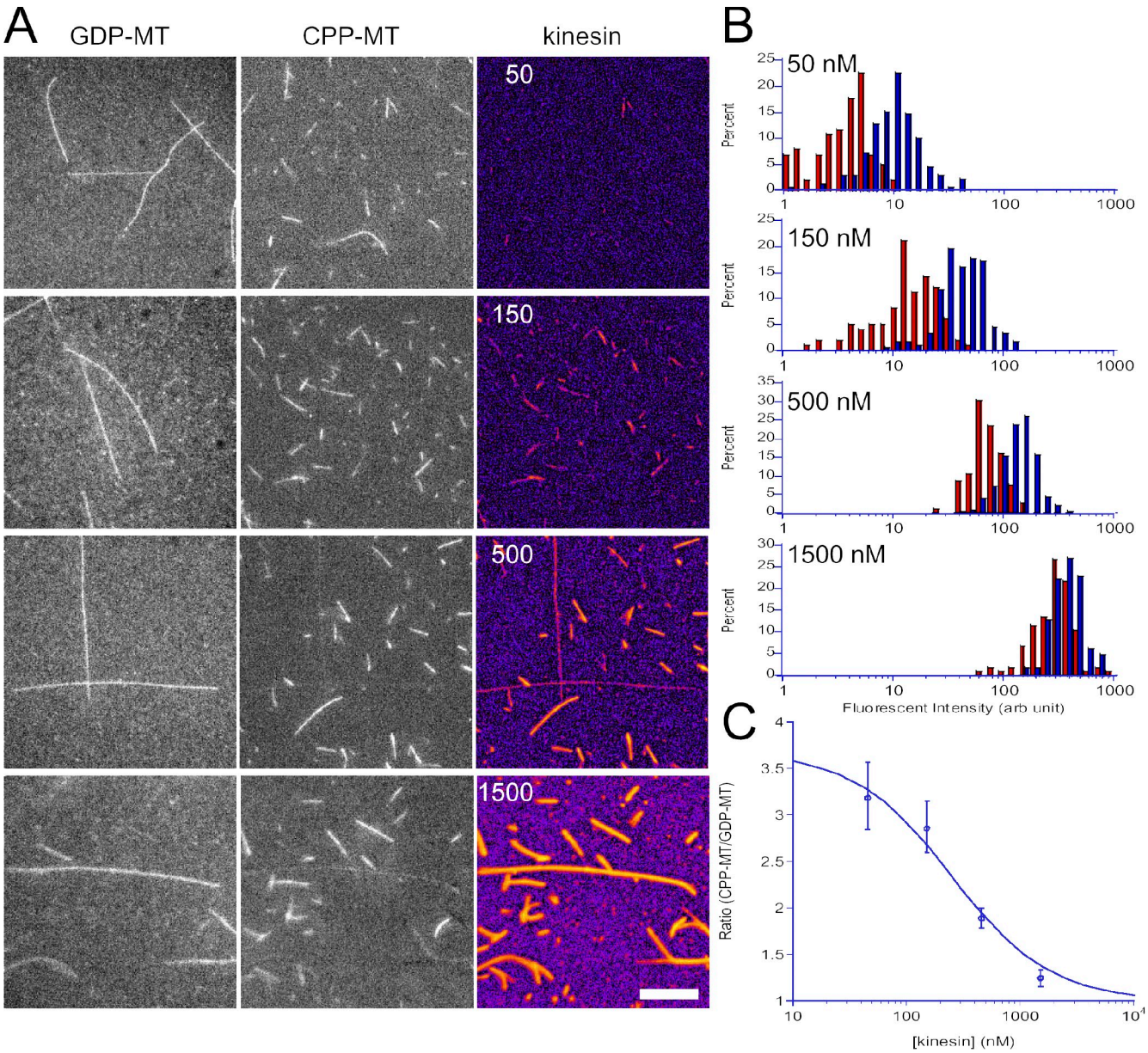

Figure 5. **In vitro binding assay.** (A) Each column of micrographs shows the GDP-MTs (labeled with Alexa Fluor 488), GMPCPP-MTs (labeled with Alexa Fluor 647), and kinesin motor domain (KIF5C, labeled with Alexa Fluor 594). Numbers in the kinesin column indicate the concentration of the kinesin motor domain (nM). Bar, 10 µm. (B) Histograms to show the fluorescence intensity of Alexa Fluor 594 channel (kinesin motor domain) bound to GDP-MTs (recognized by Alexa Fluor 488 channel signal, red) and to GMPCPP-MTs (recognized by AlexaFluor 647 channel signal, blue). The numbers in each panel show the final concentration of kinesin motor domain in the assay mixture. For each kinesin concentrations, 5–7 view fields were analyzed, which contained ~100 GDP-MTs and 150–300 GMPCPP-MTs. (C) The ratio of bound kinesin between GMPCPP-MTs and GDP-MTs, plotted against kinesin concentration. The ratio was fitted with simple binding kinetics: $\text{Ratio} = (K_{diss}^{GDP} + [\text{kinesin}]) / (K_{diss}^{CPP} + [\text{kinesin}])$, where K_{diss}^{CPP} and K_{diss}^{GDP} are the dissociation constants for GMPCPP-MTs and GDP-MTs, respectively. The mean and SEM of the same dataset as B and the best fit curve ($K_{diss}^{GDP} = 930 \pm 250$ nM and $K_{diss}^{CPP} = 250 \pm 90$ nM) are shown. The data shown are from two separate replicates of the experiment, which are representative of five replicates of the experiment.

structure of MTs in living cells. hMB11 stained not only the growing tips of MTs, but also numerous spots along the MTs in nonneuronal cells. In neurons, hMB11 preferentially stained spots along axonal MTs, which suggests that axonal MTs were abundant in spots of GTP-tubulins or tubulins with GTP-like structural features that are recognized by this antibody (GTP remnants). The present result was supported by our earlier observation of the high affinity of EB1-YFP for axonal MTs (Nakata and Hirokawa, 2003) because EB1 was recently shown to have higher affinity for GTP-MTs than for GDP-MTs (Zanic et al., 2009; Maurer et al., 2011). We showed that EB1 and hMB11 were colocalized at the single MT level (Fig. 2), which suggests that EB1 and hMB11 both recognize some structural differences between the axonal and dendritic MT lattice. Although the details of the binding sites of EB1 and the hMB11 antibody have yet to be clarified, both discriminate GTP-MTs from GDP-MTs in vitro (Dimitrov et al., 2008; Zanic et al., 2009; Maurer et al., 2011). Thus, it is likely that the structural difference between axonal and

dendritic MT lattice recognized by both EB1 and hMB11 is GTP-tubulin itself or some structure emanating from GTP-tubulin.

In addition to the axon-dominant distribution, the effect of low-dose paclitaxel (Fig. 2 C) and results from an in vitro binding assay (Fig. 5), hMB11 dynamics (Fig. 4), and super-resolution microscopy of KIF5 and hMB11 binding site (Fig. 3) together suggest that the difference between axonal and dendritic MTs recognized by hMB11 is an axonal cue for polarized transport. KIF5 moved on GMPCPP-MTs ∼30% faster than on GDP-MTs in an in vitro motility assay (Vale et al., 1994). Although our chimeric motor protein study could not specify the cue (Fig. 1), its results implicated GTP-MTs as a cue. Loop 11 of KIFs protrudes into a cleft between β-tubulin and α-tubulin (Song et al., 2001). It has been thought that GDP-tubulin and GTP-tubulin have curved and straight conformations as dimers, respectively (Müller-Reichert et al., 1998). GDP-tubulin may be constrained in a straight conformation in the MT lattice, and structural differences between GTP-tubulin and GDP-tubulin in the lattice may well exist around the intradimer cleft. There are other possible mechanisms to explain the involvement of GTP-MTs in KIF5 recruitment. Although abundant, GTP remnants are distributed as patches along the axonal MTs (Figs. 2 D and 3 A). However, there is a possibility that the GTP remnants change the MT lattice structures, which are assembled from the remnants. In such a case, in addition to the direct binding of KIF5 to GTP-MTs, the binding of KIF5 to adjacent GDP-MT segments on the same MT might be also facilitated, as described previously as cooperative binding (Skiniotis et al., 2003; Muto et al., 2005). Another possibility is that GTP-MTs could be a hot spot for posttranslational modification of MTs, and thus, GTP-MTs indirectly contribute to the KIF5 binding. However, this process alone cannot explain the results of our in vitro binding assay (Fig. 5). We cannot eliminate the possibility that GTP-MTs may act together with one or more posttranslational modifications to generate the axonal cue identified here. The relative contributions of each must await future work characterizing the structure of individual MTs, and the regulation of kinesin motor function by kinesin–MT interactions, in living neurons.

In neuronal polarity formation, one neurite grows rapidly among others and becomes an axon. The abundance of GTP-tubulin in axonal MTs may explain their stable nature, owing to the insertion of multiple rescue points as GTP remnants, which may result in a shift of axonal MTs to the growing phase. Because polarized organization of cytoskeletal and membrane proteins are both essential parts of neuronal polarity formation, their mechanisms should ultimately converge into one. Formation of GTP-MTs may be a candidate common event upstream of these mechanisms.

Materials and methods

Constructs

Chimeric constructs of mouse KIF1A and KIF5C were made to achieve the following amino acid sequences: C11K (RADSTGAEGAVLDEGANINKSLT), K11C (GSEKVSKTGAAKNINKSLSAKGTRLK), C8A (PKNKGNLAVAEHPLLGP), K8R (LDVSKTNLRVREDKNRVP), CK1 (VISALAEGTKTFIPYRDS), and SK2 (VISALAEMDSGPNKNKKKKKTDHVPYRDS; Okada and Hirokawa, 2000; Nitta et al., 2004). They were then subcloned into pYFP-N1 at the EcoRI and BamHI sites. Mouse β3-tubulin cDNA was subcloned into pYFP N1 (Homma et al., 2003).

Truncated motor study

Immediately after dissociation from 16.5-d mouse embryos, hippocampal cells were transfected with plasmids by electroporation (using a rat neuron transfection kit; Lonza) and grown on coverslip bottom dishes (Lab-Tek II; Thermo Fisher Scientific), typically for 36 h. The medium was then replaced with L-15 medium supplemented with B-27, and time-lapse data from >100 neurons were obtained using an inverted microscope (IX-72 ZDC; Olympus) equipped with an autofocus multiple-points observation system (20× objective lenses) at 37°C. Data were typically collected at 10-min intervals for 8 h.

Overexpression of hMB11-mCherry tends to cause its aggregation in cells (Dimitrov et al., 2008). We carefully controlled the expression level to avoid aggregation, and observed neurons in which hMB11-mCherry showed a cytosolic pattern.

Immunostaining

YL1/2, GT335, 6-11B-1, and Glu-tubulin (AB3201 Millipore) antibodies were used for staining of tyrosinated, polyglutaminated, acetylated, and detyrosinated tubulin. Cells were observed under a confocal laser scanning microscope (LSM-510; Carl Zeiss) equipped with 40× C-APO objective lenses (Fig. S1).

For hMB11 staining, hippocampal cells were permeabilized at 37°C in PEM (80 mM Pipes, 2 mM EGTA, and 1 mM $MgCl_2$, pH 6.9) with 10% glycerol and 0.05% Triton X-100 for 3 min. After two washes with warmed glycerol-PEM, cells were incubated with 1/200 hMB11 antibody for 15 min at 37°C in glycerol-PEM containing 0.2% BSA. After washing in PEM-glycerol (2 s, twice), cells were incubated with secondary anti–human IgG antibodies (Invitrogen) for 10 min in PEM-glycerol containing 0.2% BSA. Paclitaxel was not used during these steps (Dimitrov et al., 2008). After three final washes, cells were fixed in ice-cold methanol for 5 min and washed with PBS. HM2 was used for MAP2 staining. Cells were observed under a confocal laser scanning microscope (LSM-510; Carl Zeiss) equipped with a 40× C-APO objective lenses. For immunoelectron microscopy, cells were fixed with 2% paraformaldehyde and 0.1% glutaraldehyde for 10 min after washes in hMB11 antibody. Cells were washed and incubated with 50 mM glycine with PBS for 10 min. After blocking with BSA, cells were incubated with anti-GFP antibody (1:100; MBL) for 1 h, washed with PBS followed by TBS, pH 8.2, and incubated with 1:20 secondary antibodies conjugated with 5-nm and 10-nm colloidal gold overnight. After washing with PBS, cells were postfixed with 2% glutaraldehyde and processed for conventional EM.

Super-resolution microscopy

Images from photoactivated localization microscopy (PALM) using Dronpa and subdiffraction-resolution fluorescent imaging with ATTO dyes were combined (Betzig et al., 2006; van de Linde et al., 2009). Dronpa was provided by the Miyawaki laboratory (RIKEN Brain Science Institute, Wako, Saitama, Japan; Ando et al., 2004). Dronpa was replaced with EGFP of the GFPN1 vector (Takara Bio Inc.). To prepare secondary antibody, we conjugated anti–human antibody (Sigma-Aldrich) with ATTO 565 NHS ester (ATTO-TEC) by the standard procedure recommended by the manufacturer.

For dual-color photoswitching microscopy, hippocampal cells were transfected with cDNA for truncated KIFs-Dronpa using adenoviruses. 24–48 h after transfection, cells were incubated with hMB11 in extraction buffer (0.1 M Pipes, pH 6.8, 5 mM $MgSO_4$, 10 mM EGTA, 4% polyethylene glycol 4000, and 0.01% saponin supplemented with 5 mM AMP-PNP; Hollenbeck, 1989) for 15 min and then incubated with secondary antibody for 10 min in the same buffer. Finally, cells were fixed in cold methanol for 5 min. After the addition of 10% glucose supplemented with 10 mM glutathione, catalase, and glucose oxidase, the cells were observed using a PALM system (Carl Zeiss) equipped with 100× objective lenses, NA 1.46 (Shroff et al., 2008). Time-lapse hMB images (>16,000) were obtained with a cooled charge-coupled device (CCD) camera (Andor) with total internal reflection fluorescence (TIRF) illumination from a 561-nm laser, and Dronpa images (>16,000) were obtained with TIRF illumination from 405-nm and 489-nm lasers. To correct the drift during sampling and the chromatic shift between different fluorophores, 100-nm-diameter Au fiducial beads (BBInternational) were added to the observation buffer before super-resolution imaging. Images from two channels were aligned using fiducial beads signals common to two channels. If KIF5 or KIF1A signals were partially identified on hMB11 clusters, we considered them positive.

MT-binding assay

Tubulin was purified from porcine brains by six cycles of polymerization and depolymerization. A high-molarity Pipes buffer was used to remove

contaminating microtubule-associated proteins (Castoldi and Popov, 2003). Purified tubulin was then labeled with Alexa Fluor 488 or 647 succinimidyl ester (Invitrogen) as described previously (Desai and Mitchison, 1998). In brief, polymerized microtubules were reacted with Alexa Fluor dye in polymerization buffer (100 mM Pipes, pH 6.8, 1 mM EGTA, 1 mM $MgCl_2$, 1 mM GTP, and 10% DMSO). Labeled microtubules were collected by centrifugation through a 60% glycerol cushion. The labeled microtubules were then depolymerized with ice-cold Pipes buffer, and the supernatant was collected by centrifugation to remove aggregates and nondepolymerizing populations. Labeled tubulin was mixed with unlabeled tubulin so that ∼10% of the tubulin was labeled with Alexa Fluor dye, and was diluted to 10 µM with ice-cold polymerization buffer (80 mM Pipes, pH 6.8, adjusted with KOH, 0.8 mM EGTA, 0.8 mM MgCl2, 20% glycerol, and 0.7 mM GMPCPP or 1 mM GTP). After a 30-min incubation on ice, the mixture was clarified by centrifugation at 4°C for 30 min at 100,000 *g* using a TLA-55 rotor in a TLX ultracentrifuge (Beckman Coulter). The supernatant was warmed to 37°C to initiate polymerization. The polymerized GMPCPP-MT and GDP-MT were mixed in the prewarmed assay buffer (80 mM Pipes, pH 6.8, adjusted with KOH, 0.8 mM EGTA, 0.8 mM MgCl2, 20% glycerol, 2 mM AMP-PNP, 1 mM glucose, 0.2 mg/ml glucose oxidase, 0.04 mg/ml catalase, and 5 mM cysteamine) with the mixing ratio of 1:1:10 (CPP-MT/GDP-MT/buffer). Pre-diluted Alexa Fluor 594–labeled KIF5C monomeric motor domain (K351 in Okada and Hirokawa, 2000) was then mixed into the MT mixture with the final concentration of KIF5C motor domain at 50–1500 nM. The sample was kept 37°C to minimize depolymerization of GDP-MTs. After incubation at 37°C, the kinesin–MT mixture was spread on the cover glass and observed by epifluorescent microscopy (TE-2000E; Nikon) with a 100× Plan-Apochromat TIRF/1.45 objective lens (Nikon) and an EM CCD camera Luca (Andor Technology).

Online supplemental material

Fig. S1 shows posttranslational modification of tubulins in axons and dendrites. Fig. S2 shows the effect of HDAC6 inhibitor (trichostatin A) on truncated kinesin accumulation and tubulin acetylation. Fig. S3 shows super-resolution microscopy (dSTORM) of hMB11 staining, EB1-YFP, and truncated motor proteins. Fig. S4 shows the dynamics of truncated KIF1A and hMB11-mCherry in stage 2 neurons. Video 1 shows accumulation of CA-KIF5C to the tips of a future axon in MAP2 (−/−) hippocampal neurons in stage 2-to-3 transition. Online supplemental material is available at http://www.jcb.org/cgi/content/full/jcb.201104034/DC1.

We thank Y. Takei for the MAP2-KO mice, Y. Kanai for the anti-KIF5C antibody, and H. Sato and T. Akamatsu for technical support.

This work was supported by a grant for specially promoted research to N. Hirokawa and a global COE project grant from the Ministry of Education, Culture, Sports, Science and Technology of Japan.

Submitted: 7 April 2011
Accepted: 21 June 2011

References

Ando, R., H. Mizuno, and A. Miyawaki. 2004. Regulated fast nucleocytoplasmic shuttling observed by reversible protein highlighting. *Science*. 306:1370–1373. doi:10.1126/science.1102506

Baas, P.W., M.M. Black, and G.A. Banker. 1989. Changes in microtubule polarity orientation during the development of hippocampal neurons in culture. *J. Cell Biol.* 109:3085–3094. doi:10.1083/jcb.109.6.3085

Betzig, E., G.H. Patterson, R. Sougrat, O.W. Lindwasser, S. Olenych, J.S. Bonifacino, M.W. Davidson, J. Lippincott-Schwartz, and H.F. Hess. 2006. Imaging intracellular fluorescent proteins at nanometer resolution. *Science*. 313:1642–1645. doi:10.1126/science.1127344

Burack, M.A., M.A. Silverman, and G.A. Banker. 2000. The role of selective transport in neuronal protein sorting. *Neuron*. 26:465–472. doi:10.1016/S0896-6273(00)81178-2

Cai, D., D.P. McEwen, J.R. Martens, E. Meyhofer, and K.J. Verhey. 2009. Single molecule imaging reveals differences in microtubule track selection between Kinesin motors. *PLoS Biol.* 7:e1000216. doi:10.1371/journal.pbio.1000216

Castoldi, M., and A.V. Popov. 2003. Purification of brain tubulin through two cycles of polymerization-depolymerization in a high-molarity buffer. *Protein Expr. Purif.* 32:83–88. doi:10.1016/S1046-5928(03)00218-3

Coy, D.L., W.O. Hancock, M. Wagenbach, and J. Howard. 1999. Kinesin's tail domain is an inhibitory regulator of the motor domain. *Nat. Cell Biol.* 1:288–292. doi:10.1038/13001

Desai, A., and T.J. Mitchison. 1998. Preparation and characterization of caged fluorescein tubulin. *Methods Enzymol.* 298:125–132. doi:10.1016/S0076-6879(98)98014-4

Dimitrov, A., M. Quesnoit, S. Moutel, I. Cantaloube, C. Poüs, and F. Perez. 2008. Detection of GTP-tubulin conformation in vivo reveals a role for GTP remnants in microtubule rescues. *Science*. 322:1353–1356. doi:10.1126/science.1165401

Dotti, C.G., and G. Banker. 1991. Intracellular organization of hippocampal neurons during the development of neuronal polarity. *J. Cell Sci. Suppl.* 15:75–84.

Friedman, D.S., and R.D. Vale. 1999. Single-molecule analysis of kinesin motility reveals regulation by the cargo-binding tail domain. *Nat. Cell Biol.* 1:293–297. doi:10.1038/13008

Friedman, J.R., B.M. Webster, D.N. Mastronarde, K.J. Verhey, and G.K. Voeltz. 2010. ER sliding dynamics and ER-mitochondrial contacts occur on acetylated microtubules. *J. Cell Biol.* 190:363–375. doi:10.1083/jcb.200911024

Goslin, K., and G. Banker. 1999. Rat hippocampal neurons in low-density culture. *In* Culturing Nerve Cells, G. Banker and K. Goslin, editors. MIT Press, Boston. 251–281.

Hammond, J.W., D. Cai, and K.J. Verhey. 2008. Tubulin modifications and their cellular functions. *Curr. Opin. Cell Biol.* 20:71–76. doi:10.1016/j.ceb.2007.11.010

Hammond, J.W., C.F. Huang, S. Kaech, C. Jacobson, G. Banker, and K.J. Verhey. 2010. Posttranslational modifications of tubulin and the polarized transport of kinesin-1 in neurons. *Mol. Biol. Cell*. 21:572–583. doi:10.1091/mbc.E09-01-0044

Hirokawa, N., and R. Takemura. 2005. Molecular motors and mechanisms of directional transport in neurons. *Nat. Rev. Neurosci.* 6:201–214. doi:10.1038/nrn1624

Hirokawa, N., S. Niwa, and Y. Tanaka. 2010. Molecular motors in neurons: transport mechanisms and roles in brain function, development, and disease. *Neuron*. 68:610–638. doi:10.1016/j.neuron.2010.09.039

Hollenbeck, P.J. 1989. The distribution, abundance and subcellular localization of kinesin. *J. Cell Biol.* 108:2335–2342. doi:10.1083/jcb.108.6.2335

Homma, N., Y. Takei, Y. Tanaka, T. Nakata, S. Terada, M. Kikkawa, Y. Noda, and N. Hirokawa. 2003. Kinesin superfamily protein 2A (KIF2A) functions in suppression of collateral branch extension. *Cell*. 114:229–239. doi:10.1016/S0092-8674(03)00522-1

Jacobson, C., B. Schnapp, and G.A. Banker. 2006. A change in the selective translocation of the Kinesin-1 motor domain marks the initial specification of the axon. *Neuron*. 49:797–804. doi:10.1016/j.neuron.2006.02.005

Konishi, Y., and M. Setou. 2009. Tubulin tyrosination navigates the kinesin-1 motor domain to axons. *Nat. Neurosci.* 12:559–567. doi:10.1038/nn.2314

Marcos, S., J. Moreau, S. Backer, D. Job, A. Andrieux, and E. Bloch-Gallego. 2009. Tubulin tyrosination is required for the proper organization and pathfinding of the growth cone. *PLoS ONE*. 4:e5405. doi:10.1371/journal.pone.0005405

Maurer, S.P., P. Bieling, J. Cope, A. Hoenger, and T. Surrey. 2011. GTPgammaS microtubules mimic the growing microtubule end structure recognized by end-binding proteins (EBs). *Proc. Natl. Acad. Sci. USA*. 108:3988–3993. doi:10.1073/pnas.1014758108

Müller-Reichert, T., D. Chrétien, F. Severin, and A.A. Hyman. 1998. Structural changes at microtubule ends accompanying GTP hydrolysis: information from a slowly hydrolyzable analogue of GTP, guanylyl (alpha,beta) methylenediphosphonate. *Proc. Natl. Acad. Sci. USA*. 95:3661–3666. doi:10.1073/pnas.95.7.3661

Muto, E., H. Sakai, and K. Kaseda. 2005. Long-range cooperative binding of kinesin to a microtubule in the presence of ATP. *J. Cell Biol.* 168:691–696. doi:10.1083/jcb.200409035

Nakata, T., and N. Hirokawa. 2003. Microtubules provide directional cues for polarized axonal transport through interaction with kinesin motor head. *J. Cell Biol.* 162:1045–1055. doi:10.1083/jcb.200302175

Nakata, T., S. Terada, and N. Hirokawa. 1998. Visualization of the dynamics of synaptic vesicle and plasma membrane proteins in living axons. *J. Cell Biol.* 140:659–674. doi:10.1083/jcb.140.3.659

Nitta, R., M. Kikkawa, Y. Okada, and N. Hirokawa. 2004. KIF1A alternately uses two loops to bind microtubules. *Science*. 305:678–683. doi:10.1126/science.1096621

Okada, Y., and N. Hirokawa. 2000. Mechanism of the single-headed processivity: diffusional anchoring between the K-loop of kinesin and the C terminus of tubulin. *Proc. Natl. Acad. Sci. USA*. 97:640–645. doi:10.1073/pnas.97.2.640

Reed, N.A., D. Cai, T.L. Blasius, G.T. Jih, E. Meyhofer, J. Gaertig, and K.J. Verhey. 2006. Microtubule acetylation promotes kinesin-1 binding and transport. *Curr. Biol.* 16:2166–2172. doi:10.1016/j.cub.2006.09.014

Rosenfeld, S.S., B. Rener, J.J. Correia, M.S. Mayo, and H.C. Cheung. 1996. Equilibrium studies of kinesin-nucleotide intermediates. *J. Biol. Chem.* 271:9473–9482. doi:10.1074/jbc.271.2.688

Shroff, H., H. White, and E. Betzig. 2008. Photoactivated localization microscopy (PALM) of adhesion complexes. *Curr. Protoc. Cell Biol.* Chapter 4:Unit 4.21.

Skiniotis, G., T. Surrey, S. Altmann, H. Gross, Y.-H. Song, E. Mandelkow, and A. Hoenger. 2003. Nucleotide-induced conformations in the neck region of dimeric kinesin. *EMBO J.* 22:1518–1528. doi:10.1093/emboj/cdg164

Song, Y.H., A. Marx, J. Müller, G. Woehlke, M. Schliwa, A. Krebs, A. Hoenger, and E. Mandelkow. 2001. Structure of a fast kinesin: implications for ATPase mechanism and interactions with microtubules. *EMBO J.* 20:6213–6225. doi:10.1093/emboj/20.22.6213

Song, A.H., D. Wang, G. Chen, Y. Li, J. Luo, S. Duan, and M.M. Poo. 2009. A selective filter for cytoplasmic transport at the axon initial segment. *Cell*. 136:1148–1160. doi:10.1016/j.cell.2009.01.016

Takei, Y., J. Teng, A. Harada, and N. Hirokawa. 2000. Defects in axonal elongation and neuronal migration in mice with disrupted tau and map1b genes. *J. Cell Biol.* 150:989–1000. doi:10.1083/jcb.150.5.989

Tapia, M., F. Wandosell, and J.J. Garrido. 2010. Impaired function of HDAC6 slows down axonal growth and interferes with axon initial segment development. *PLoS ONE*. 5:e12908. doi:10.1371/journal.pone.0012908

Vale, R.D., C.M. Coppin, F. Malik, F.J. Kull, and R.A. Milligan. 1994. Tubulin GTP hydrolysis influences the structure, mechanical properties, and kinesin-driven transport of microtubules. *J. Biol. Chem.* 269:23769–23775.

van de Linde, S., U. Endesfelder, A. Mukherjee, M. Schüttpelz, G. Wiebusch, S. Wolter, M. Heilemann, and M. Sauer. 2009. Multicolor photoswitching microscopy for subdiffraction-resolution fluorescence imaging. *Photochem. Photobiol. Sci.* 8:465–469. doi:10.1039/b822533h

Zanic, M., J.H. Stear, A.A. Hyman, and J. Howard. 2009. EB1 recognizes the nucleotide state of tubulin in the microtubule lattice. *PLoS ONE*. 4:e7585. doi:10.1371/journal.pone.0007585